In Vitro Testing and Comparison of Additively Manufactured Polymer Impellers for the CentriMag Blood Pump

Kai von Petersdorff-Campen,* Jonas Abeken,† Diane de Zélicourt,† Vartan Kurtcuoglu,† Mirko Meboldt,* and Marianne Schmid Daners*.

Additive manufacturing (AM) is an effective tool for accelerating knowledge gain in development processes, as it enables the production of complex prototypes at low cost and with short lead times. In the development of mechanical circulatory support, the use of cheap polymer-based AM techniques for prototype manufacturing allows more design variations to be tested, promoting a better understanding of the respective system and its optimization parameters. Here, we compare four commonly used AM processes for polymers with respect to manufacturing accuracy, surface roughness, and shape fidelity in an aqueous environment. Impeller replicas of the CentriMag blood pump were manufactured with each process and integrated into original pump housings. The assemblies were tested for hydraulic properties and hemolysis in reference to the commercially available pump. Computational fluid dynamic simulations were carried out to support the transfer of the results to other applications. In hydraulic testing, the deviation in pressure head and motor current of all additively manufactured replicas from the reference pump remained below 2% over the entire operating range of the pump. In contrast, significant deviations of up to 620% were observed in hemolysis testing. Only the replicas produced by stereolithography showed a nonsignificant deviation from the reference pump, which we attribute to the low surface roughness of parts manufactured thereby. The results suggest that there is a flow-dependent threshold of roughness above which a surface strongly contributes to cell lysis by promoting a hydraulically rough boundary flow. *ASAIO Journal* 2020; XX:00–00.

Key Words: additive manufacturing, 3D printing, mechanical circulatory support, blood pumps, in vitro testing, hydraulic characterization, hemolysis, CentriMag

From the *Product Development Group Zurich, Department of Mechanical and Process Engineering, ETH Zurich, Zurich, Switzerland and †The Interface Group, Faculty of Medicine, Institute of Physiology, University of Zurich, Zurich, Switzerland

Submitted for consideration November 2019; accepted for publication in revised form May 2020.

Disclosure: The authors have no potential conflicts of interest with respect to the research, authorship, and/or publication of this research.

Supplemental digital content is available for this article. Direct URL citations appear in the printed text, and links to the digital files are provided in the HTML and PDF versions of this article on the journal's Web site (www.asaiojournal.com).

Correspondence: Marianne Schmid Daners, Product Development Group Zurich, Department of Mechanical and Process Engineering, ETH Zurich, CLA G 21.1, Tannenstrasse 3, 8092 Zurich, Switzerland. Email: marischm@ethz.ch.

DOI: 10.1097/MAT.0000000000001220

Additive manufacturing (AM) has become an indispensable tool in research and development because it offers many advantages, *e.g.*, in the production of prototypes.[1] However, the application of AM is only feasible if the results of tests with printed prototypes are not affected by the manufacturing method itself and can be transferred to the final product, for which other materials and manufacturing processes might be used. In addition to the basic mechanical properties and biocompatibility, the limited manufacturing accuracy and generally increased surface roughness of AM parts are of particular concern. In the development of mechanical circulatory support (MCS) devices with, *e.g.*, complex impeller geometries AM is useful for the quick validation of computer simulations and extensive testing of design variations.[2–7] Few studies have investigated the applicability of AM in MCS devices, but deviations in hydraulic properties and increased *in vitro* hemolysis have been observed.[8,9] However, those studies did not cover the broad range of new and continuously improving AM processes and materials. In this study, we have therefore investigated the applicability of four state-of-the-art AM processes for polymers for *in vitro* testing of hydraulic properties and hemolysis using the CentriMag blood pump impeller as an application example. Associations between the part properties of the additively manufactured impellers with the deviation from the original impeller in hydraulic and hemolysis testing were evaluated.

Materials and Methods

Integration into the CentriMag Pump

The CentriMag is a commercial extracorporeal centrifugal blood pump that can operate at pump speeds (n) of 1000 to 5500 revolutions per minute (rpm) with flow rates (Q) up to 10 L/min. It can, therefore, be used both as ventricular assist device (VAD) (pressure head H ≈ 110 mmHg, Q ≈ 5 L/min, $n = 2350$ rpm, "VAD-like operating point") and for extracorporeal membrane oxygenation (ECMO) (H ≈ 360 mmHg, Q ≈ 5 L/min, $n = 4050$ rpm, "ECMO-like operating point"). It has a magnetically levitated impeller and provides a low blood damage profile that is manifested in very low hemolysis levels (normalized index of hemolysis (NIH) <3 mg/100 l).[10] It consists of a control unit, a motor unit and a disposable pump head (**Figure 1**). Its hydraulic characteristics are most commonly described by the relation of H with Q, which is represented by performance curves at constant n in so-called HQ diagrams. The motor current (I) needed to achieve a given Q can similarly be illustrated in so-called IQ diagrams.

The geometry of the impeller body was reconstructed from an optical 3D scan of the CentriMag impeller and additively manufactured by an external supplier (1zu1 Prototypen GmbH

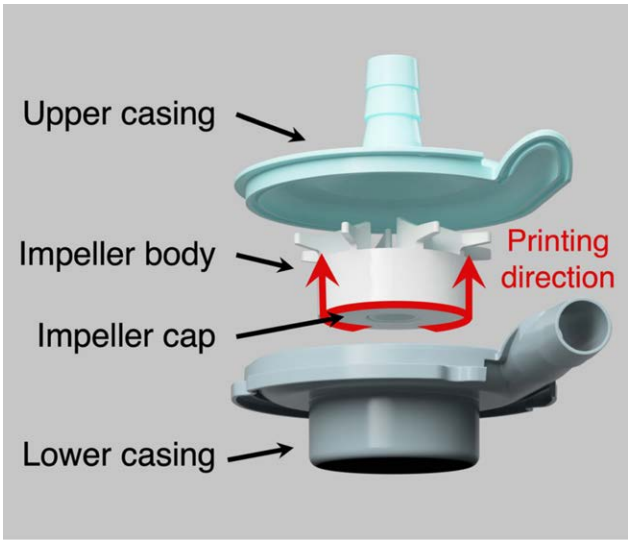

Figure 1. Schematic of the assembly of the CentriMag pump head. In this study, the impeller body was additively manufactured along its rotation axis ("Printing direction").

& Co KG, Dornbirn, Austria). The ISO 10993 certified biocompatible glue Loctite 4061 (Henkel, Düsseldorf, Germany) was used to assemble the impeller replicas with additional impeller and housing parts into functional pump heads as shown in **Figure 1** (parts provided by Thoratec Switzerland GmbH [part of Abbott], Zürich, Switzerland).

Fabrication with Additive Manufacturing Processes

Four different AM machines for macroscopic hard-polymer objects were selected for the production of replicas, namely selective laser sintering (SLS), multi-jet fusion (MJF), material jetting (MJ), and stereolithography (SLA). The popular fused deposition modeling process was not used in this study because the print resolution was insufficient to produce the thin parts (<0.7 mm) of the CentriMag impeller. Widely used equipment was selected from companies that are among the five largest manufacturers of industrial printers[11] based on the highest printing resolution in their category although striving for coverage of a range of printing approaches. Although all machines can process biocompatible materials, standard materials were used for reasons of availability. The AM process and material specifications, shown in **Table 1**, were collected from the manufacturers as well as the literature. A detailed description of the printing processes is provided in Supplemental Digital Content 1, http://links.lww.com/ASAIO/A518. The impellers were printed along the axis of rotation (**Figure 1**). In addition, three disc-shaped specimens for water absorption tests were printed at 0°, 45°, and 90° relative to the printing direction. Only the process-specific minimal post-processing was performed.

Characterization of AM Parts

Because pump parts must maintain their shape in an aqueous environment, water absorption tests were carried out on disc-shaped specimens (L × W × T: 20×10×1.5 mm^3) according to the ASTM D-57098 standard. The dimensions and mass of the specimens were measured before and after submersion in deionized water for a period of 24 h at 37°C. After aqueous exposure, the external geometry of the assembled impellers was scanned using a GOM-ATOS compact optical metrology system (GOM GmbH, Braunschweig, Germany) and the generated 3D surfaces were compared with the scan of the reference impeller in the GOM Inspect Professional v7.5 software (GOM GmbH). The deviation of the AM impellers from reference was measured at 78,000–187,000 surface points per impeller with a resolution of 0.01 mm. Two metrics were used to assess printing accuracy: The fraction of surface points in a ±0.1 mm tolerance and the mean deviation of surface points to the reference (mean deviation). For each AM process, the accuracy was determined for three replicas from different printing batches

Table 1. Manufacturing Processes

Manufacturing category	Conventional	Powder bed fusion	Powder bed fusion	Photopolymerization	Photopolymerization
Manufacturing process	Injection Molding (IM)	Selective laser sintering (SLS)	Multi-jet fusion (MJF)	Material jetting (MJ)	Stereolithography (SLA)
Machine	n.a.	Formiga P110 Velocis	Jet Fusion 3D 4200	Objet Eden 350V	Viper Si2
Material	Makrolon 2858	PA12	PA12	Fullcure RDG 720	Prototherm
Company	Thoratec Switzerland GmbH, Zurich, Switzerland	EOS, München, Germany	HP, Palo Alto, CA, USA	Stratasys, Eden Prairie, MN, USA	3D Systems, Rock Hill, SC, USA
Support	n.a.	n.a.	n.a.	Part fully embedded in gel-like support material SUP705	Support rods from build material
Biocompatibility*	USP Class VI	USP Class VI	USP Class VI	n.a.	n.a.
Layer Thickness (mm)*	n.a.	0.1	0.08	0.016	0.05
x–y Resolution (DPI)*	n.a.	n.a.	1,200 DPI	600 DPI	n.a.
Laser spot size (μm)*	n.a.	<500	n.a.	n.a.	75 ± 15
Density (g/cm^3)*	1.02	1	1.01	1.18–1.19	1.15
Elastic modulus (MPa)*	2,400	1,600	1,800	2,000–3,000	3,500
Tensile strength (MPa)*	66	43	48	50–65	70
Elongation at break (%)*	50	14	15–20	15–25	3
Manufacturing costs per impeller (USD)†	n.a.	30	24	70	235

*Data provided by manufacturers.
†As offered by 1zu1 Prototypen GmbH & Co KG, Dornbirn, Austria.

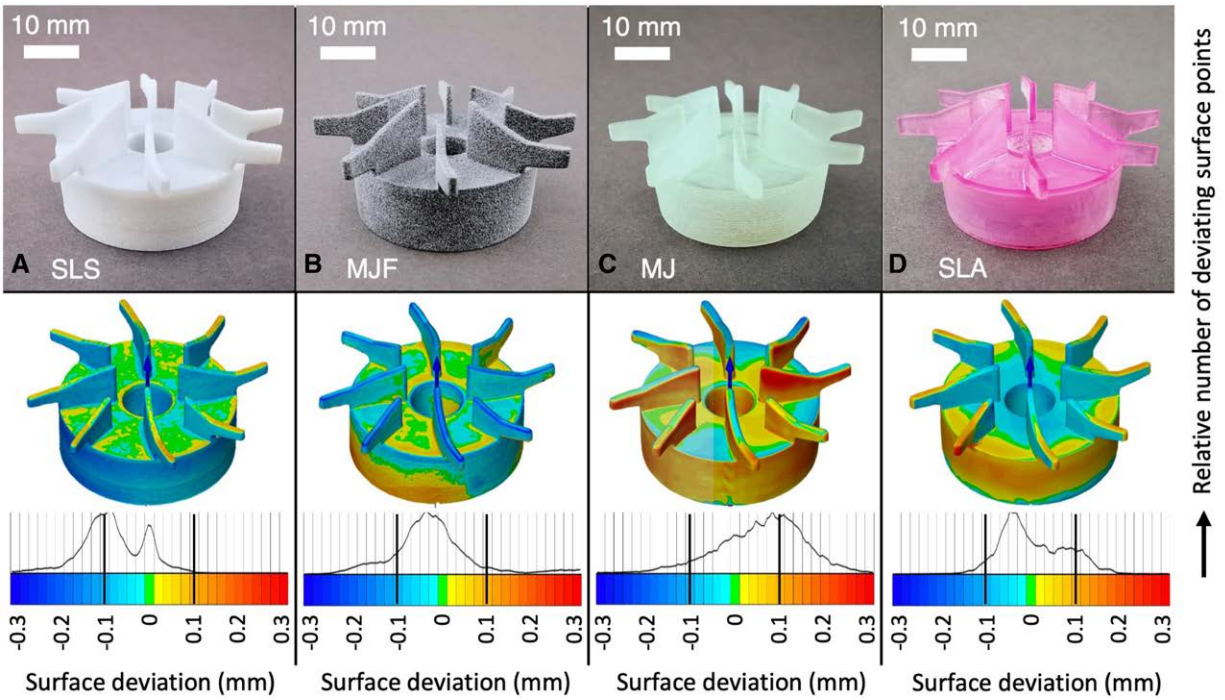

Figure 2. Photographs (top row) and 3D scans (bottom row) of the replicas manufactured by (A) SLS, (B) MJF, (C) MJ, and (D) SLA, see **Table 1** for details. The 3D scans are colored according to local nominal-actual comparisons with the reference impeller. The degree and distribution of the deviation are shown in histograms, in which the relative number of surface points used for comparison are plotted according to the deviation. The color bars depict the respective surface deviations. MJ, material jetting; MJF, multi-jet fusion; SLA, stereolithography; SLS, selective laser sintering.

to assess the reproducibility of the AM processes. The surface roughness of the impellers was measured in twelve separate areas ($250 \times 375\ \mu m^2$) at locations both parallel and orthogonal to the printing direction using a laser scanning confocal microscope (VK-X200, Keyence, Osaka, Japan) with a 10X objective and a resolution of 1 nm. The roughness parameters S_a (arithmetical mean deviation of surface profile) and R_z (maximum peak-valley distance) were extracted using the Multi-File Analyzer Software (Keyence, Osaka, Japan). Because vertical surfaces make up the largest part of the impeller, only the roughness of these surfaces is considered in the analysis.

Hydraulic Characterization

The hydraulic measurements of the pump assemblies were performed using a mock circulatory loop for static testing. A 40 wt.% glycerine/water mixture was used as the working fluid, which according to Cheng *et al.*[12] has a viscosity of 3.5 cP at the working temperature of 23ºC. The flow rate was measured with a clamp-on ultrasonic flow probe (Sonoflow CO.55, Sonotec Ultraschallsensorik Halle GmbH, Halle, Germany). The pressures were measured directly at the pump inlet and outlet with absolute pressure transducers (Type 528, Huba Control AG, Würenlos, Schweiz). In addition, the motor current (I) was measured. The measurement precision of the test bench was determined by five repeated measurements of the reference assembly at a pump speed of 4,000 rpm. Details on the setup can be found in the Supplemental Digital Content 1, http://links.lww.com/ASAIO/A518. All parameters were measured at about 180 operating points per impeller for n and Q in the range of 1,000–5,500 rpm and 0–10 L/min, respectively. All motor current data were normalized by the current of the reference pump at the VAD-like operating point ($I_{ref,VAD}$).

Hemolysis

Fresh bovine blood was collected from the local slaughterhouse and anticoagulated with 10 vol.% of 0.109 M sodium citrate solution. The hematocrit (Hct) was adjusted to 30 ± 2% by diluting with phosphate-buffered saline. The pH of the blood was checked to range between 7.4 and 7.6. The diluted blood was filtered using blood filters (Dideco Kids D130, LivaNova PLC, London, UK). Five identical recirculating flow loops were constructed according to the ASTM F1841-19 guidelines for *in vitro* hemolysis assessment in continuous flow blood pumps.[13] A detailed description of the setup can be found in Supplemental Digital Content 1, http://links.lww.com/ASAIO/A518.

Each hemolysis test was performed with all five pump assemblies in parallel with 500 ml each of blood from the same animal. Blood samples of 2 ml were collected at hourly intervals for 6 h and the free plasma hemoglobin fHb was measured using the Harboe method.[14] The NIH was calculated according to Eq. 1 with the increase of fHb during one sampling interval ΔfHb (mg/l), the remaining circuit volume V (l), the adjusted hematocrit Hct (%), the flow rate Q (L/min) and the sampling time T (min). The tests were repeated three times with blood from different animals for both the VAD-like and the ECMO-like operating conditions resulting in 18 NIH values per replica.

$$\mathrm{NIH\,(mg/100L)} = \Delta\mathrm{fHb} \cdot \mathrm{V} \cdot \frac{100 - \mathrm{Hct}}{100} \cdot 100 / (\mathrm{Q} \cdot \mathrm{T}) \qquad (1)$$

Computational Fluid Dynamic Simulation

Computational fluid dynamic (CFD) simulations were performed to determine the range of wall shear stresses (WSS) and successively laminar sublayer thickness on the impeller. The simulations were conducted on the original pump geometry assuming smooth no-slip walls. The CFD model was based on a previously described setup[12] and is thus only summarized here. A more detailed description is provided in Supplemental Digital Content 1, http://links.lww.com/ASAIO/A518. Both VAD- and ECMO-like operating conditions were analyzed by prescribing a pressure head of 105 mmHg at 2350 rpm for VAD operation and 350 mmHg at 4050 rpm for ECMO, respectively. WSS histograms were extracted every five time-steps and afterward averaged more than 10 impeller rotations. The laminar sublayer height δ_v was calculated according to Eq. 2, with the dimensionless wall distance y^+, the dynamic viscosity μ, the WSS τ_W, and the density ρ. The laminar sublayer thickness $\delta_{v,95}$ corresponding to the 95th percentile WSS was chosen as a representative lower limit of sublayer thickness on the impeller.

$$\delta_v = y^+ \cdot \mu \Big/ \sqrt{\tau_W \cdot \rho} \tag{2}$$

Statistical Analysis

To model the hydraulic behavior, the general additive model function of the R package mgcv[16] and a spline regression model were used. The regression included terms for Q, n, and the interaction between these two terms (Eq. 3). For each impeller, these terms were obtained separately. The models had high explanatory power ($R^2_{adj} > 0.99$).

$$\text{Target (H or I)} \sim s(Q) + s(n) + te(Q, n) + s(n,\ \text{impeller}) + s(Q,\ \text{impeller}) + te(Q, n,\ \text{impeller}) \tag{3}$$

Estimates and confidence intervals for deviations from the reference at specific operating points were calculated using the variance–covariance matrix of the model coefficients. Furthermore, the root mean square error (RMSE) of the deviation at grid points in the entire speed/flow plane was calculated to assess the global deviation from the reference. T-tests were conducted to compare the mean values of hemolysis testing. *p*-values below 0.05 were considered as indicators of statistical significance unless indicated otherwise.

Results

Printing process and manufacturing accuracy

Per manufacturing method, three replicas were produced in separate batches. All replicas had sufficient mechanical integrity and accuracy for assembly and pump operation. The analysis of the 3D scans is shown in **Figure 2** for one set of impellers. The fraction of surface points with a ±0.1 mm tolerance and the mean deviation are presented in **Table 2** as metrics for accuracy and reproducibility. The SLA replica had the smallest mean deviation overall (+5 µm), although the SLS and MJ replicas showed a clear tendency to undersize (–81 µm) or oversize (+57 µm), respectively. The SLA and MJF impeller showed the smallest (±0.5%) and largest (±5.6%) variation in the ±0.1 mm tolerance between batches, respectively. The cost of manufacturing was the lowest for the powder-based processes (SLS and MJF) and about 10 times higher for SLA (**Table 1**).

Surface roughness

Exemplary laser scanning microscopy images and color-coded topography of areas with the surface normal perpendicular to the axis of rotation are shown in **Figure 3**. Surface features resulting from the layer-wise manufacturing can be

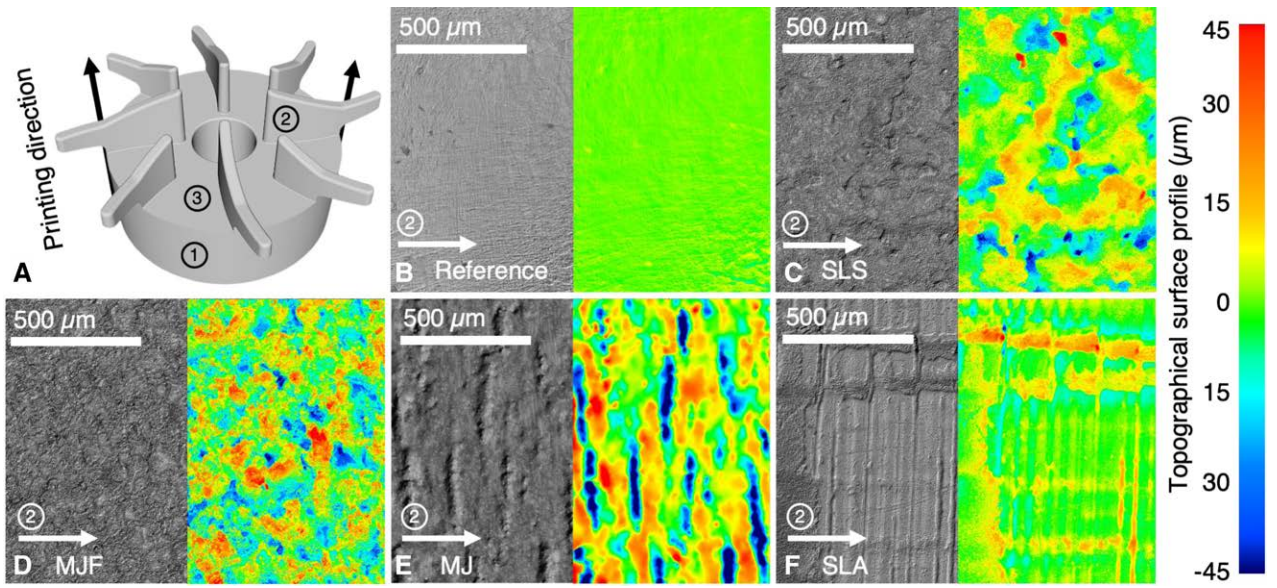

Figure 3. Surface roughness measurements of the CentriMag impellers. (A) Indication of the printing direction and the locations of surface roughness measurements (1: sidewall of impeller body, 2: sidewall impeller blade, 3: top side of impeller sidewall impeller blade). (B)–(F) Exemplary laser scanning microscopy images (left) and color-coded topography (right, from blue = lower to red = higher) at the sidewall of an impeller blade of the (B) reference impeller and the replicas manufactured by (C) SLS, (D) MJF, (E) MJ, and (F) SLA (**Table 1**). MJ, material jetting; MJF, multi-jet fusion; SLA, stereolithography; SLS, selective laser sintering.

Table 2. Characterization of Additively Manufactured Specimens

	Reference	SLS	MJF	MJ	SLA
Fraction of surface points in ±0.1 mm tolerance (%)*	96	65	80	71	92
Reproducibility of ±0.1 mm tolerance (%)†	±1.3	±3.3	±5.6	±4.2	±0.5
Mean deviation from reference impeller (µm)*	+13	−81	−18	+57	+5
Surface roughness S_a (µm)‡	0.8 ± 0.5 (v)	7.8 ± 0.9 (v)	11.7 ± 0.5 (v)	14.1 ± 1.2 (v)	5.4 ± 0.9 (v)
	0.2 ± 0.1 (h)	5.7 ± 0.2 (h)	12.0 ± 1.2 (h)	4.7 ± 0.5 (h)	0.3 ± 0.1 (h)
	0.7 ± 0.4 (a)	7.4 ± 0.8 (a)	11.8 ± 0.6 (a)	12.1 ± 1.1 (a)	4.3 ± 0.7 (a)
Surface roughness R_z (µm)‡	14.5 ± 5.4 (v)	67.8 ± 15.5 (v)	89.6 ± 17.8 (v)	127.2 ± 13.6 (v)	26.9 ± 8.9 (v)
	4.4 ± 1.9 (h)	59.9 ± 27.1 (h)	109.9 ± 21.35 (h)	72.3 ± 14.3 (h)	5.0 ± 2.2 (h)
	12.4 ± 4.7 (a)	66.1 ± 18.0 (a)	94.0 ± 18.6 (a)	115.6 ± 13.7 (a)	22.3 ± 7.5 (a)
Water absorption (wt.%)	0.3§	0.56¶	0.71¶	2.5¶	1.13¶

*Measured for the impeller geometries used for *in vitro* testing as shown in **Figure 2**.
†Determined from three impellers per manufacturing method that were printed in different batches ‡Measured on four 250 × 375 µm² areas separate on vertical (v) and horizontal (h) surfaces as shown in **Figure 3a** and averaged (a) according to the fraction of the respective surface type (v-to-h ratio of 3.73).
§According to the manufacturer.
¶Measured on disk-shaped specimens.

seen for the SLA and MJ replica. The mean roughness values at different locations of the impellers are given in **Table 2**. All replicas had higher surface roughness than the reference. Although the SLA replica had smooth surfaces with a maximum roughness of up to seven times that of the reference, the other replicas showed 10–60 times rougher surfaces than the reference. The roughness of the vertical and horizontal surfaces was similar for the powder-based printing processes (MJF and SLS), although the horizontal surfaces were up to 18 times smoother for the resin-based printing processes (MJ and SLA).

Water Absorption

None of the additively manufactured discs showed a water absorption relevant for the application in this study. The largest water uptake was seen for the MJ discs with approximately 2.5 wt.% (**Table 2**). Changes in length, width, thickness, or warping could not be observed.

Hydraulic Characterization

The test bench precision was determined to ±1.19 mmHg in H, ±0.15 L/min in Q, and ±0.01 A in I. A statistical spline regression model was used to analyze the hydraulic behavior of the impellers. The modeled pressure heads of the reference were 109.8 ± 1 mmHg and 359.5 ± 1 mmHg at the VAD-like and ECMO-like operating points, respectively. The modeled relations of H and normalized motor current ($I/I_{ref,VAD}$) with Q are shown in **Figure 4** in VAD-like and ECMO-like operating conditions.

Apart from an off-set along the H and I axis, the curves had the same shape, such that the dependency of Q was similar for all impellers. The replica assemblies showed an average deviation from the reference of 1.7% and 1.9% in H and I, respectively. The local and overall differences between the assemblies are presented in **Figure 5**. **Figure 6** shows the deviation in I plotted against the deviations in H at all measured data points. The MJF impeller showed the largest global deviation in H and I with an RMSE of 17 mmHg and 0.065 A, respectively. At the VAD-like operating point, the deviation in H and I of the SLS replica was the smallest among all replicas. Interestingly, at the ECMO-like operating point, the SLS impeller generated lower H over the whole Q range than the reference (on average −5.5 mmHg, **Figure 6**), whereas the impellers manufactured by MJ and SLA showed the smallest deviation in H with less than 1.5 mmHg.

A positive correlation (r = 0.88) of H and $I/I_{ref,VAD}$ was found, indicating that impellers generating higher pressure also require higher motor currents (**Figure 6**).

Hemolysis

The results of the hemolysis testing are presented in **Figure 7**. The SLA replica performed closest to the reference with a

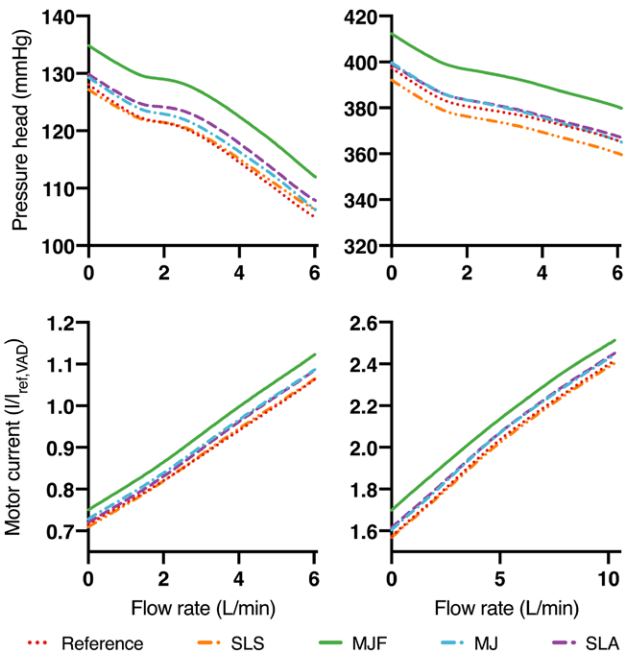

Figure 4. Relation of pressure head (H) and normalized motor current ($I/I_{ref,VAD}$) to flow rate (Q) fitted with spline regression models for the CentriMag reference assembly and additively manufactured replica assemblies at stationary conditions of 2350 (VAD-like) and 4,050 rpm (ECMO-like). ECMO, extracorporeal membrane oxygenation; VAD, ventricular assist device.

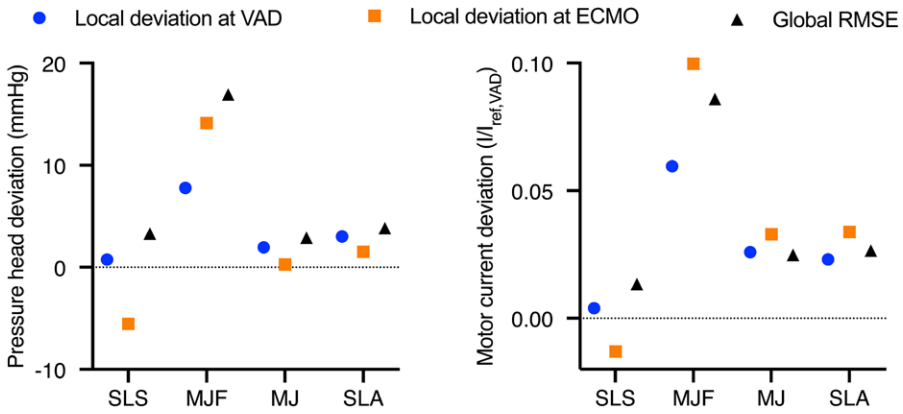

Figure 5. Comparison of the deviation from the reference in pressure head (H) and normalized motor current ($I/I_{ref,VAD}$) of different replica assemblies. Both the deviation at the VAD-like and ECMO-like operating points as well as the global deviation are shown (represented by the root mean square error (RMSE) of deviations at grid points over the entire n–Q range). ECMO, extracorporeal membrane oxygenation; VAD, ventricular assist device.

statistically not significant increase of NIH of approximately 30% (VAD: $p = 0.55$, ECMO: $p = 0.93$). The SLS, MJ, and MJF replicas showed significantly higher NIH values compared with the reference with an increase of up to 500% at the VAD-like ($p = 7.7 \cdot 10^{-5}$, $p = 0.011$, $p = 0.012$) and up to 620% at the ECMO-like operating point ($p = 3.1 \cdot 10^{-4}$, $p = 1.2 \cdot 10^{-5}$, $p = 5.5 \cdot 10^{-3}$). The NIH showed a positive correlation with the impeller roughness S_a, with a stronger correlation at the ECMO-like operating point (VAD: corr. = 0.72, ECMO: corr. = 0.84). The generated H of the reference was 105 ± 1 mmHg and 350 ± 1 mmHg at the VAD-like and ECMO-like operating points, respectively.

CFD Simulations

The simulated Q was 4.96 L/min at the VAD-like and 5.00 L/min at the ECMO-like operating point. Histograms of WSS action on the impeller surface are shown in **Figure 8**. At the VAD-like operating point, the average WSS was 47 Pa, and the 95th percentile of experienced WSS was 132 Pa. The WSS values at the ECMO-like operating point were about twice as high, with an average of 99 Pa and the 95th percentile of 277 Pa. The effect of pressure-induced forces on the calculated rotor torque exceeded the effect of shear-induced forces by an order of magnitude at both the VAD-like and the ECMO-like operating point. The representative laminar sublayer height at the VAD-like and ECMO-like operating condition is calculated to be $\delta_{v,95,VAD} = 47.0$ µm and $\delta_{v,95,ECMO} = 32.5$ µm, respectively.

Discussion

In this study, four CentriMag impellers were manufactured with different AM processes, characterized with respect to part quality, hydraulic behavior as well as hemolysis, and compared with each other. We elaborate on the causes for observed deviations from the original injection-molded impeller and discuss the transferability of our results to other applications.

Manufacturing and Pump Operation

At the VAD-like operating point, the smallest gap between the cylindrical impeller body and the housing is approximately

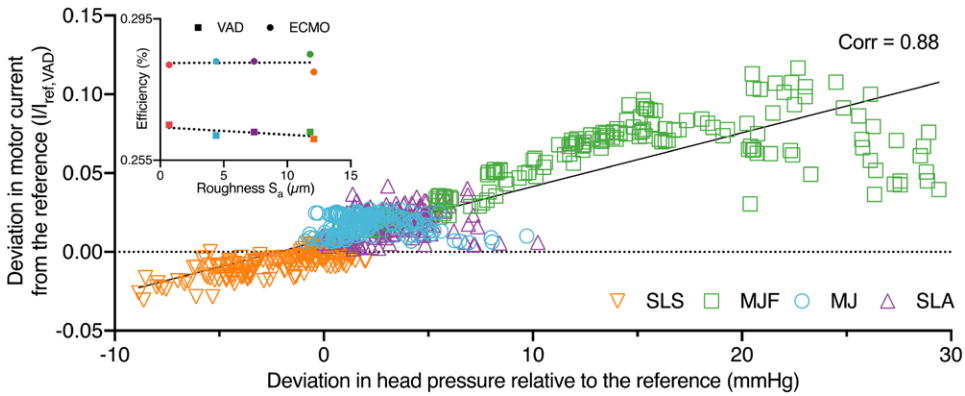

Figure 6. Deviations from the reference in pressure head (H) and normalized motor current ($I/I_{ref,VAD}$) of the replica assemblies from the reference assembly plotted against each other at all measured data points. The data shows a large positive correlation of H and $I/I_{ref,VAD}$ with a correlation coefficient of 0.88. The subplot illustrates that surface roughness does not have a strong influence on efficiency. VAD, ventricular assist device.

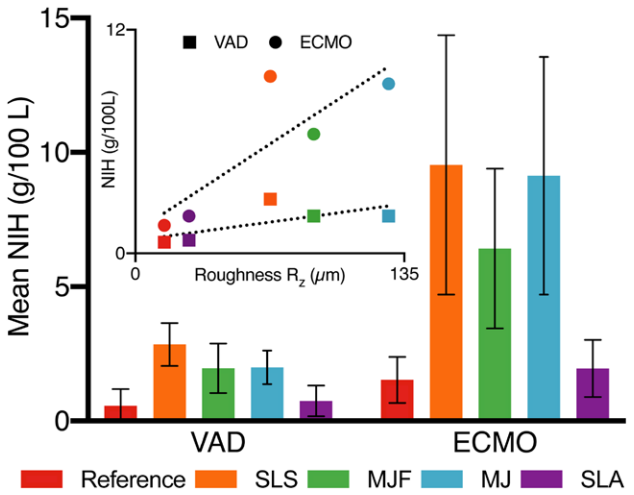

Figure 7. Comparison of the normalized indices of hemolysis (NIH) of the reference and replica assemblies at a VAD-like (~105 mmHg, 5 L/min, 2350 rpm) and ECMO-like (~350 mmHg, 5 L/min, 4050 rpm) operating point. The subplot illustrates the positive correlation between hemolysis and surface roughness with stronger expression at the ECMO-like operating point. ECMO, extracorporeal membrane oxygenation; VAD, ventricular assist device.

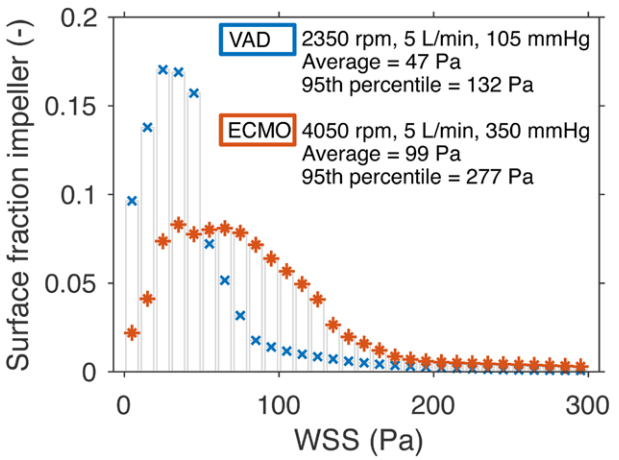

Figure 8. Simulated wall shear stress (WSS) distribution on the impeller surface during VAD-like and ECMO-like operation of the CentriMag pump. At the VAD-like and ECMO-like operating point the 95th percentile of experienced WSSs is 132 Pa and 277 Pa, respectively. ECMO, extracorporeal membrane oxygenation; VAD, ventricular assist device.

550 μm. In comparison, the mean deviations of the replicas from the reference geometry in this gap are considerable at –130 μm (SLS) and +120 μm (MJ). As the surface roughness of most replicas was high and potentially relevant for *in vitro* testing, additional post-processing could be considered. The surface of the MJ replica was particularly rough because it had been fully embedded in support material. If the use of support can be avoided, smoother surfaces may be expected. Deformation of replicas with concomitant friction contact, as observed by Nishida *et al.*,[9] was not an issue in the used magnetic levitation system with large gaps, but might become relevant in different applications with smaller tolerances.

Hydraulic Performance and Hemolysis

Because the rotor torque is dominated by pressure-induced and not shear-induced forces, changes in the bulk flow are necessary to produce noticeable deviations in hydraulic performance. Therefore, no influence of near-wall phenomena is expected. Accordingly, the impellers show almost no difference in efficiency despite a drastic difference in surface roughness (**Figure 6**). The more likely cause for changes in bulk flow is larger geometric deviations of the replicas. However, no systematic correlations could be seen between the metrics for manufacturing accuracy applied here and differences in H and I. For example, the MJ impeller showed one of the largest mean deviations, but performed closest to the reference among all impellers. A more complex investigation of the influences of geometric deviation at specific locations seems to be required.

The drastically increased NIH of most replicas is likely to be caused by surface roughness through increased friction and shear at the impeller surface. This is evident in the positive correlation of the NIH with surface roughness (**Figure 7**). The effect is pronounced at the ECMO-like operating point, which can be explained by the higher pump speed and the concomitant higher WSS at this operating point (**Figure 8**) that at the VAD-like operation. Although the roughness of the SLA replica is already two to seven times higher than that of the reference impeller, a significant increase in hemolysis is only observed in the other replicas, which have more than 10 times greater surface roughness than the reference. This may suggest that there is a threshold for surface roughness below which no additional hemolysis is induced, as previously observed by Maruyama *et al.*[17] One possible explanation for such a threshold value is the transition from a hydraulically smooth to a hydraulically rough boundary layer, caused by a surface roughness that exceeds the flow-dependent height of the laminar sublayer. A surface with an equivalent sand roughness smaller than the laminar sublayer thickness would be assumed to be hydraulically smooth and without influence on the rest of the boundary layer and main flow.[18] Using the results of the CFD analysis, we can compare the computed laminar sublayer thickness with the roughness value R_z (**Table 2**) as a good approximation for the equivalent sand roughness[19] and judge whether the surface roughness is expected to impact the main flow and consequently hemolysis. Only the SLA roughness ($R_z = 26.9 \pm 8.9$ μm) remains below the calculated lower limit of the laminar sublayer height $\delta_{v,95}$, whereas all other replicas would exceed the threshold value in both the VAD-like ($\delta_{v,95,VAD} = 47.0$ μm) and ECMO-like ($\delta_{v,95,ECMO} = 32.5$ μm) operating condition. This is consistent with the observed results. However, it remains unclear why the SLS impeller caused higher or equal hemolysis levels than the MJ and MJF replicas at lower surface roughness. Therefore, additional effects not addressed in this study are likely to play a role, such as particular damaging surface patterns, material properties, or the formation of distinct flow fields.

Transferability to Other Applications

When considering transferability to other applications, a distinction must be made between purely hydrodynamic and hemolysis tests. All four AM processes investigated appear to be suitable for hydraulic testing. As the shape of the HQ and IQ curves were similar among all impellers, even for the MJF impeller with the

biggest discrepancy from the reference of all replicas, a correction for deviations from injection-molded parts could be performed by off-setting the respective curve in H or I. As also stated by Chan *et al.*[8] SLS provides a good trade-off between manufacturing costs and performance in hydraulic testing. For hemolysis testing, however, SLA seems to be the only suitable method, possibly because only this method can produce surfaces that can be considered hydraulically smooth under the given conditions.

Considering the manufacturing costs, it seems reasonable to use the low-cost SLS process for the production of hydraulic prototypes and to use the more expensive SLA processes for the production of selected designs for hemolysis tests. The presented results apply only to the investigated combinations of AM processes and materials and might not hold if other materials are processed on the same printers.

According to boundary layer theory, the height of the laminar sublayer is inversely proportional to the square root of the WSS. Given our previously stated hypothesis on the sublayer-dependent impact of surface roughness, we expect our results to be transferable to other applications as long as the WSSs are of a similar magnitude to the current study. A change in sublayer thickness with different WSSs or fluids could render the surfaces of the SLA method hydraulically rough or, vice-versa, make other methods such as SLS usable for hemolysis tests.

Experimental Limitations

The *in vitro* characterization of the replicas was performed on one impeller of each AM process. However, we have shown that the deviation in manufacturing accuracy between replicas of the same AM process is small compared with the process differences, which suggests replicability of the experiments. By the nature of the experiments, the impeller design and the printing method were confounded. In statistical terms, the different behavior of another design manufactured with the same process cannot be excluded.

Conclusion

The use of additively manufactured parts for *in vitro* testing of blood pumps is feasible but manufacturing inaccuracy and surface roughness have to be considered. Nonsystematic manufacturing inaccuracies were identified as a major factor before the surface roughness for deviation of AM replicates in hydraulic performance. In contrast, surface roughness appeared to have a substantial influence on the results when testing hemolysis. The AM parts did not show any deformation or disintegration when exposed to an aqueous environment. It was concluded that all AM processes considered here can be used to manufacture prototypes for purely hydrodynamic testing, although only the SLA process is capable of manufacturing parts that perform similar to injection molded parts in hemolysis testing. The use of AM parts in a different pump system might require additional validation, especially if the range of WSSs present in the CentriMag pump is exceeded.

Acknowledgment

The authors gratefully acknowledge the financial support by the Stavros Niarchos Foundation (SNF) and by the Swiss National Science Foundation through NCCR Kidney.CH. We thank the Thoratec Switzerland GmbH, Zurich, Switzerland (part of Abbott) for the financial support and for providing the CentriMag pump systems used in this study. Furthermore, the authors would like to thank Florian Mauz for his help in carrying out the experiments. This work is part of the Zurich Heart project under the umbrella of "Hochschulmedizin Zürich".

References

1. Fontana F, Klahn C, Meboldt M: Value-driven clustering of industrial additive manufacturing applications. *J Manuf Technol Manag* 30: 366–390, 2019
2. Wiegmann L, Boës S, de Zélicourt D, et al: Blood pump design variations and their influence on hydraulic performance and indicators of hemocompatibility. *Ann Biomed Eng* 46: 417–428, 2018.
3. Thamsen B: A two-stage rotary blood pump design to reduce blood trauma. *Artif Organs* 39: 651–659, 2016.
4. Kennington JR, Frankel SH, Chen J, *et al*: Design optimization and performance studies of an adult scale viscous impeller pump for powered Fontan in an idealized total cavopulmonary connection. *Cardiovasc Eng Technol* 2: 237–243, 2011.
5. Throckmorton AL, Kapadia JY, Chopski SG, et al: Numerical, hydraulic, and hemolytic evaluation of an intravascular axial flow blood pump to mechanically support Fontan patients. *Ann Biomed Eng* 39: 324–336, 2011.
6. Okamoto E, Hashimoto T, Inoue T, Mitamura Y: Blood compatible design of a pulsatile blood pump using computational fluid dynamics and computer-aided design and manufacturing technology. *Artif Organs* 27: 61–67, 2003
7. Rajenthirakumar D, Jagadeesh KA: Analysis of interaction between geometry and efficiency of impeller pump using rapid prototyping. *Int J Adv Manuf Technol* 44: 890–899, 2009.
8. Chan WK, Wong YW, Chua CK, Lee CW, Feng C: Rapid manufacturing techniques in the development of an axial blood pump impeller. *Proc Inst Mech Eng Part H J Eng Med* 217: 469–475, 2003
9. Nishida M, Negishi T, Sakota D, et al: Properties of a monopivot centrifugal blood pump manufactured by 3D printing. *J Artif Organs* 19: 322–329, 2016.
10. Chan CH, Pieper IL, Hambly R, et al: The CentriMag centrifugal blood pump as a benchmark for *in vitro* testing of hemocompatibility in implantable ventricular assist devices. *Artif Organs* 39: 93–101, 2015.
11. Context 3D Printing Report: CONTEXT AM3DP Report 2019. Available at: https://www.contextworld.com/new-metal-3d-printers-have-industry-on-pace-for-25%25-higher-end-printer-growth-in-2019. Accessed July 18, 2019.
12. Cheng NS: Formula for the viscosity of a glycerol-water mixture. *Ind Eng Chem Res* 47: 3285–3288, 2008.
13. ASTM Standard F1830-19. *Standard Practice for Collection and Preparation of Blood for Dynamic In Vitro Evaluation of Hemolysis in Blood Pumps*. West Conshohocken, PA, ASTM International, 2006. doi: 10.1520/F1830-19. Available at: www.astm.org.
14. Harboe M: A method for determination of hemoglobin in plasma by near-ultraviolet spectrophotometry. *Scand J Clin Lab Invest* 11: 66–70, 1959.
15. Wiegmann L, Thamsen B, de Zélicourt D, et al: Fluid dynamics in the HeartMate 3: Influence of the artificial pulse feature and residual cardiac pulsation. *Artif Organs* 43: 363–376, 2019.
16. Wood SN, Pya N, Säfken B: Smoothing parameter and model selection for general smooth models *J Am Stat Assoc* 111: 1548–1563, 2016.
17. Maruyama O, Nishida M, Yamane T, Oshima I, Adachi Y, Masuzawa T: Hemolysis resulting from surface roughness under shear flow conditions using a rotational shear stressor. *Artif Organs* 30: 365–370, 2006.
18. Schlichting H, Gersten K: *Boundary-Layer Theory*. Springer, 2016.
19. Adams T, Grant C, Watson H: A Simple algorithm to relate measured surface roughness to equivalent sand-grain roughness *Int J Mech Eng Mechatronics* 1, 2012